Specificity and Catalysis of Uracil DNA Glycosylase. A Molecular Dynamics Study of Reactant and Product Complexes with DNA†

Ning Luo, Ernest Mehler, and Roman Osman*

Department of Physiology and Biophysics, Mount Sinai School of Medicine of the City University of New York, One Gustave L. Levy Place, New York, New York 10029

Received February 4, 1999; Revised Manuscript Received May 6, 1999

ABSTRACT: The structure of uracil DNA glycosylase (UDG) in complex with a nonamer duplex DNA containing a uracil has been determined only in the product state. The reactant state was constructed by reattaching uracil to the deoxyribose, and both complexes were studied by molecular dynamics simulations. Significant changes in the positions of secondary structural elements in the enzyme are induced by the hydrolysis of the glycosidic bond. The simulations show that the specificity of the uracil pocket in the enzyme is largely retained in both complexes with the exception of Asn-204, which has been identified as a residue that contributes to discrimination between uracil and cytosine. The hydrogen bond between the amide group of Asn-204 and O_4 of uracil is disrupted by fluctuations of the side chain in the reactant state and is replaced by a hydrogen bond to water molecules trapped in the interior of the protein behind the uracil binding pocket. The role of two residues implicated by mutation experiments to be important in catalysis, His-268 and Asp-145, is clarified by the simulations. In the reactant state, His-268 is found 3.45 ± 0.34 Å from the uracil, allowing a water molecule to form a bridge to O_2. The environment in the enzyme raises the pK_a value of His-268 to 7.1, establishing a protonated residue for assisting in the hydrolysis of the glycosidic bond. In agreement with the crystallographic structure, the DNA backbone retracts after the hydrolysis to allow His-268 to approach the O_2 of uracil with a concomitant release of the bridging water molecule and a reduction in the pK_a to 5.5, which releases the proton to the product. The side chain of Asp-145 is fully solvated in the reactant state and H-bonded through a water molecule to the 3′-phosphate of uridine. Both the proximity of Asp-145 to the negatively charged phosphate and its pK_a of 4.4 indicate that it cannot act as a general base catalyst. We propose a mechanism in which the bridging water between Asp-145 and the 3′-phosphate accepts a proton from another water to stabilize the bridge through a hydronium ion as well as to produce the hydroxide anion required for the hydrolytic step. The mechanism is consistent with known experimental data.

One of the most frequent occurrences of DNA damage is the spontaneous deamination of cytosine, which is produced at a rate of a few hundred uracil bases in a cell per day (*1*). The resulting U·G mismatch base pairing, if not repaired, may lead to mutations (*2*). To protect the integrity of DNA, the ubiquitous and highly conserved DNA repair enzyme uracil DNA glycosylase (UDG)[1] (*3*−*7*) initiates the first step of base excision repair by catalyzing the hydrolysis of the N−$C_{1'}$ glycosidic bond of uracil. The resulting apyrimidinic (AP) site is the target of AP-endonuclease (*8*), and the nicked backbone is processed by deoxyribophosphodiesterase to remove the deoxyribose and the 5′-phosphate group (*9*). The damaged DNA strand is then repaired by DNA polymerase which inserts the correct base opposite the orphan nucleotide (*10*), and finally, the backbone is reinstated by a DNA ligase (*11*). Recent crystallographic work provided important information about the nature of these enzymes as well as about the specific interactions with damaged DNA in various stages of repair (*12*).

The important biological activity of UDG derives from a very high specificity for uracil in DNA and from a very large enhancement of the rate of glycosidic bond hydrolysis. The crystal structures of human (*5*) and herpes simplex virus UDG (*13*) have been determined, and their three-dimensional structures are very similar. The crystal structure of a double-mutant UDG in a complex with a uracil-containing DNA has also been determined recently (*14*), and it provides important insights into the nature of the specificity of the uracil binding pocket. One of the interesting features revealed by the structure shared with other DNA repair enzymes is a flipped nucleotide. The structure shows that the uracil is flipped out through the major groove and Leu-272, which has been replaced in the complex by Arg, fills the gap formed by the flipped-out nucleotide. Recently, several additional structures of the wild-type (wt) UDG and a Leu272Ala mutant in a complex with several DNAs have been determined crystallographically (*15*), reaffirming the structural

† This work was supported in part by U.S. Public Health Service Grant CA 63317 (R.O.) and NSF Grant DBI-9732684 (E.M.).

* To whom correspondence should be addressed: Department of Physiology and Biophysics, Box #1218, Mount Sinai School of Medicine, New York, NY 10029. Telephone: (212) 241-5609. Fax: (212) 860-3369. E-mail: osman@inka.mssm.edu.

[1] Abbreviations: UDG, uracil DNA glycosylase; MUG, mismatch-specific DNA glycosylase; MD, molecular dynamics; r-complex, reactant state of the UDG−DNA complex; p-complex, product state of the UDG−DNA complex.

10.1021/bi990262h CCC: $18.00
Published on Web 06/25/1999

details of the previous structure. In addition to the DNA with a U·G mismatch, the structure with a U·A base pair has been determined, both exhibiting a flipped-out structure with a hydrolyzed glycosidic bond of uracil. The mutant enzyme Leu272Ala exhibits an interesting structure in a complex with a flipped-out abasic site and a rearranged sugar in a β-conformation.

Several groups in the binding pocket that accommodates the flipped-out uracil form a network of hydrogen bonds with uracil. Specifically, the crystal structures show that Asn-204 forms two hydrogen bonds to the O_4 and N_3H of uracil, presumably defining the preference for uracil over cytosine. However, although the mutation Asn204Asp lowers the selectivity of the enzyme (as determined from k_{cat}/K_M) for a uracil-containing DNA by a factor of 50 000, the mutant enzyme selectivity for cleaving a cytosine is lower by a factor of 147 than for hydrolyzing a uracil in DNA (*16*). Furthermore, the mutation affects k_{cat} more than K_M, suggesting that the role of Asn-204 is not only in recognition but also in catalysis. The side chain of Tyr-147 is in van der Waals contact with the C_5 of uracil, presenting a steric exclusion for the 5-methyl group of thymine. Mutation Tyr147Phe changes very little the characteristics of the enzyme; however, mutation Tyr147Ala reduces the selectivity of the enzyme by a factor of 87 500, and as described before, the selectivity of the mutant enzyme toward a thymine-containing DNA is worse than for uracil by a factor of 29. Thus, while UDG does not remove thymine or cytosine from DNA, the residues in the binding pocket not only establish a binding preference but also play a role in catalysis. UDG does not remove a 3′-terminal uracil because the minimal UDG substrate is pd(UN)p (*17*). In fact, the 3′-phosphate to deoxyuridine is essential for binding and catalysis (*18*).

On the basis of the crystal structures, several enzymatic mechanisms have been proposed in spite the fact that the enzyme−DNA complex is actually that of the products of the glycosylase reaction. In the complex, the uracil is positioned approximately 3.5 Å away from the 1′-α-hydroxydeoxyribose, confirming that the glycosidic bond has been hydrolyzed. Two critical structural elements have been proposed to play a catalytic role in the glycosylase action. One is the general base catalysis activating a water molecule by Asp-145 to produce the desired nucleophile. In the complex, this residue is hydrogen bonded to a water molecule and is in the vicinity of the glycosidic bond. The other element is the general acid and/or electrostatic effect of His-268, which stabilizes the negative charge that develops on the uracil in the course of hydrolysis and thus must be protonated. These specific catalytic roles of Asp-145 and His-268 are supported by mutational experiments, but no direct evidence exists about the specific role of these groups. Of more concern is the extrapolation from the structures of enzyme−product complexes about the nature of the transition state. Since enzymes lower the barrier for the catalytic step, the transition state resembles the enzyme−substrate complex more than the enzyme−product state (*19*). Consequently, the suggestions regarding the role of various residues in the enzymatic catalysis on the basis of the crystal structures is speculative since it represents an attempt to reconstruct the catalytic reaction in the opposite direction and assumes that the enzyme−substrate complex will have properties similar to those of the enzyme−product form.

In this study, we focus on the properties of the active site of UDG, which contribute to substrate specificity and catalysis. We have reconstructed the enzyme−substrate complex, the reactant state, and describe results of molecular dynamics (MD) simulations of the UDG−DNA complex in both the reactant and the product states. The global structure and the properties of the enzyme−substrate complex are significantly different from those of the enzyme−product form. The analysis of specific interactions between UDG and DNA leads to a better understanding of the basis for DNA selectivity. The properties of two essential catalytic residues, Asp-145 and His-268, and especially the presence of several waters in the vicinity of the active site sugget a new mechanism for the catalytic action of UDG.

MATERIALS AND METHODS

Two structures have been prepared for this investigation: the enzyme−substrate complex, r-complex, and the enzyme−product complex, p-complex. The initial structure of the p-complex of UDG−DNA was constructed from the crystallographic coordinates kindly provided by J. Tainer. First, the mutations in the crystal structure were reverted to the wild-type residues: Asn-145 → Asp and Arg-272 → Leu. The two residues, Asp-145 and Leu-272, were relaxed by local minimization to relieve close contacts while keeping the rest of the complex fixed. In the crystal structure of the p-complex, the DNA contains overhang bases at both ends in its sequence. To improve the stability of the MD simulation, the two unpaired bases on both ends of the DNA were removed to yield a duplex with the sequence d(GGGUG-GCTT). In this structure, the uracil base is already cleaved and the sugar is in the 1′-α-hydroxy form. The initial structure of the r-complex of UDG−DNA was constructed from the structure of the p-complex produced by a long simulation (see below). The glycosidic bond was reconnected with the required removal of the hydrogen on N_1 of uracil and the 1′-hydroxy group of the deoxyribose. The bond distance was gradually reduced from 3.5 Å found in the p-complex to 1.5 Å with constrained MD simulation of 50 ps at 300 K in five steps, before the equilibration stage described below.

To ensure proper protonation states of the ionizable groups, we have computed the pK_a values for all the titratable groups in free and complexed UDG. These were calculated by expressing the deprotonation equilibrium in a protein with the help of the following thermodynamic cycle (*20*−*22*)

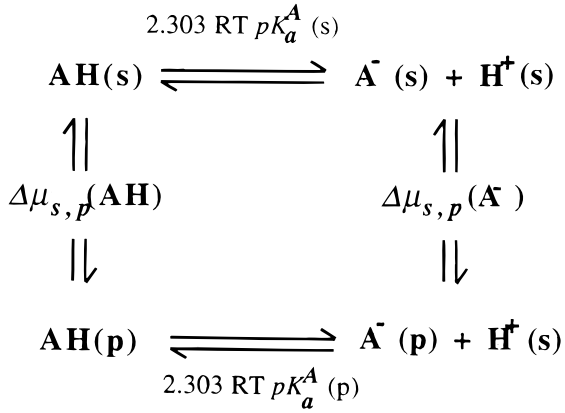

where $\Delta\mu$ is the change in chemical potential on transferring titratable group AH (or A^-) from water into the protein. From the scheme, the pK_a of group A in the protein, pK_a^A(p), can be expressed in terms of the pK_a in the model solvent (i.e., water), pK_a^A(s), and the additional changes in free energy that arise when the titratable group is transferred from water into the protein. Here only the electrostatic contributions are considered, and pK_a^A(p) is calculated from the relation

$$pK_a^A(p) = pK_a^A(s) + (w_A^{int} + \Delta w_A^{tr})/2.303RT$$

where w_A^{int} is the interaction free energy of the charged group in the field of all the other groups in the protein and Δw_A^{tr} is the change in self-energy on transferring the group from water to the protein. The two free energy terms were calculated using a new self-consistent electrostatic free energy approach based on screened Coulomb potentials (*23*). In this approach, the distribution of the ionization charge over the atoms of the titratable groups is determined variationally to optimize the total electrostatic free energy, and it includes an accounting of the local environment around each protonatable moiety (for details, see ref *24*). The method has been applied to a database of more than 100 pK_a values, and the rms difference between the calculated and measured values is around 0.5 pH unit (*24*).

The values of the model pK_a in water were as follows: N-terminus, 7.5; C-terminus, 3.8; His, 6.3; Glu, 4.4; Asp, 4.0; Tyr, 10.0; Lys, 10.4; and Arg, 12.0. The partial charges and group structures of the amino acid residues are those defined in the PAR19 topology file of CHARMM (*25*), while the partial charges of the neutral forms of the titratable groups were taken from the PAR22 (*26*, *27*) topology files. The solvent accessible surface areas required for the calculation of the transfer term were evaluated with CHARMM using a probe radius of 1.0 Å. Ionic strength was accounted for using a Debye screening term (*28*). Several histidines (His-115, His-148, and His-189) have been determined to be charged and not to depend on the nature of the complex. His-268 was the only residue whose protonation state changed from the r- to the p-complex. The decision about the δ or ϵ tautomer of the neutral histidine side chain was made on the basis of the polarity of the microenvironment of the N_δ and N_ϵ atoms.

The complexes were solvated by a periodic hexagon of water with a height of 62 Å and an edge of 40.4 Å, with eight sodium counterions to neutralize the entire system. The solvated r- and p-complexes were heated to 300 K and then equilibrated for 200 ps. After equilibration, a MD production run of 1 ns at a constant volume and energy (NVE) was performed on the p-complex and 1.2 ns for the r-complex. The trajectory of the r-complex is 200 ps longer than that of the p-complex to ensure that the small perturbation introduced by connecting the glycosidic bond at U was fully equilibrated. The standard deviation in temperature fluctuation during the production period is about 1.6−1.7 K. All simulations were carried out with CHARMM24. The step size was 2 fs, and the trajectory was recorded every 0.1 ps. The nonbonded interaction cutoff was 11.0 Å. The nonbonded interaction list and the solvent image of the water hexagon were updated every 20 fs. Even though the simulations were carried out under constant energy conditions, the total energy shows a slow upward drift of 2.2−2.8%/ns. These drifts are small and should not affect the simulation structures in a significant way.

RESULTS AND DISCUSSION

Structures of the Complexes. The simulations conducted on the r- and p-complexes serve two roles. One is to assess the effect of crystal packing forces on the structure of the complex, and the other is to investigate the changes in the structure and properties of the constructed substrate−enzyme complex (r-complex) compared to those of the product−enzyme complex (p-complex). Since the simulation of the p-complex was initiated from the X-ray structure, the evolution of the structure during the simulation represents in part the replacement of mutated residues with those in the wild-type enzyme: Asn-145 → Asp and Arg-272 → Leu. It also represents the replacement of crystal packing forces with an aqueous environment as well as the approximations introduced by the force field used in the simulation. The r-complex, however, was constructed from the equilibrated p-complex, and therefore, the changes in its structure during the simulation should reflect the effect of reconnecting the glycosidic bond between the sugar and the uracil. Regardless of the starting point in the two simulations, they reach an apparent stable structure after a brief equilibration run as indicated by the protein backbone rms deviation from the initial structures which stabilizes at approximately 1 Å. Subsequently, a slow change in the rms deviation brings the value to approximately 1.5 Å at about 500 ps. Thereafter, the rms deviation of the entire system (DNA and protein) remains essentially flat. This behavior suggests that the trajectories for both forms of the enzyme reach a relatively stable situation with small changes occurring over time.

A comparison of the averaged structure of the p-complex to the X-ray structure was limited to the protein because of the uncertainties in the DNA coordinates in the X-ray structure. The comparison shows that the overall rms deviation for backbone atoms is 1.27 Å and for all heavy atoms 1.99 Å. To examine the origin of the structural changes, the rms deviations from the X-ray structure for each residue in the p-complex are shown in Figure 1A (top). Clearly, only a limited number of residues deviate by more than 2 Å, and deviations that exceed 1 Å are mostly localized to specific regions of the protein. The amino (N) and the carboxy (C) termini, which have no specific secondary structures to maintain local stability in the protein, exhibit large deviations. Helices α_1 and α_2 that follow the N-terminus and helix α_8 that precedes the C-terminus also exhibit large deviations, possibly for the same reason as the N- and C-termini. Most other secondary structural elements that are packed against each other maintain a small rms deviation with the exception of α_6 and α_7 that exhibit deviations in excess of 2 Å. An examination of the placement of these helices in the protein shows that α_6 is surrounded on one side by α_1 and α_2 and on the other by α_7. Furthermore, Asp-227 in α_6 forms a salt bridge with Lys-252 in α_7. The movement of α_1 and α_2, possibly induced by the release of crystallographic packing forces, produces a shift in the position of α_6, which drags with it α_7 through the Asp-227···Lys-252 ionic interaction. The other regions with large changes are the loops that connect the secondary structural elements, i.e., the loops between β_1 and α_4 (residues 144−167), between α_4 and α_5 (residues 181−192), between β_2

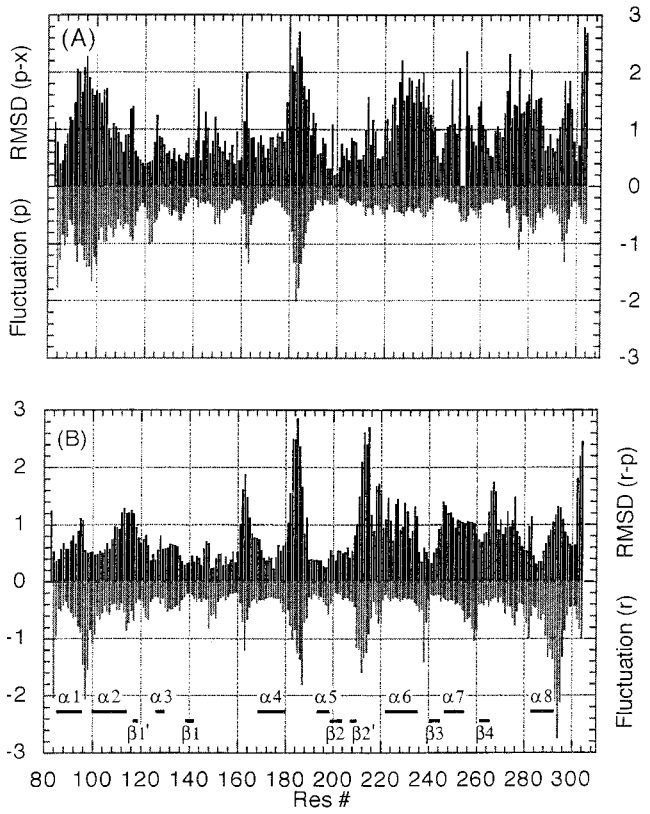

FIGURE 1: Residue fluctuations around average of the UDG−DNA complex (bottom part of each graph) derived from the simulation of the p-complex (A) and the r-complex (B) compared to the rms difference (top part of each graph) between the average structure of the p-complex and the X-ray crystallographic structure (A) and between the average structures of the r-complex and the p-complex (B).

and α_6 (residues 205−221), and between β_4 and α_8 (residues 267−282). The large deviations in the loops are associated with considerable flexibility of the backbone, as demonstrated in the plot of the fluctuations around the average structure of the p-complex shown in Figure 1A (bottom). Thus, it appears that the structures of the α_6 and α_7 helices and of the loops in the crystal are determined by packing forces, which disappear in the aqueous environment in the simulations leading to the observed structural changes, while the effects of the double reverse mutation Asn-145 → Asp and Arg-272 → Leu from the crystal structure to our p-complex are mainly local.

A similar comparison of the protein structures of the r- and p-complexes shows that the overall rms deviation between the two averaged structures for the backbone atoms is only 1.05 Å and for all heavy atoms 1.42 Å. Although the structures are very similar, there are distinct local changes, shown in Figure 1B, that suggest a strong correlation between flexible loops (Figure 1B, bottom) and large rms deviations between the two structures (Figure 1B, top). However, helices α_6 and α_7 and the loop that connects β_4 with α_8 show considerable change in spite of the fact that their flexibility is quite low. Here the comparison of the structures has to take into account the fact that the DNA structure has changed significantly due to the reconstruction of the glycosidic bond between the sugar and the uracil in the r-complex. The effect of reconnecting uracil to the DNA backbone produces several changes in the DNA (see below), which are subsequently transmitted to the protein. The rms fluctuations around the average structure of DNA residues, excluding the two base pairs at both ends of the helix, are below 1 Å in both the r- and p-complexes. They are consistently smaller than the rms differences of these residues between the r- and p-compelxes. For the DNA strand in contact with the protein, the rms differences are in the range of 1.0−1.5 Å, while for the opposite strand, they are around 2 Å. This suggests that the changes in DNA structure from the r- to the p-complex are due to the change in the glycosidic bond rather then due to DNA fluctuations. The backbone of the DNA interacts with the protein at two serines: Ser-169 at the top of helix α_4 and Ser-247 at the top of helix α_7. The interaction is illustrated on an excerpt of the structures of the r- and p-complexes of UDG with DNA shown in Figure 2. Ser-169 interacts with the phosphate of the flipped-out uracil, which upon the breaking of the glycosidic bond moves somewhat and shifts the position of the α_4 helix by a small amount. At the other attachment point, Ser-247 interacts with the phosphate of Cyt-7, where the change in the position of the phosphate due to the cleavage of the glycosidic bond is quite large. The transmission of the change to the α_7 helix can be seen in Figure 2 as represented by the movement of Lys-252, which through an ionic interaction with Asp-227 in helix α_6 induces a rotational motion in the α_6 helix. This can be seen in Figure 2 as well as in the helical periodicity of the rms deviation shown in the top graph of Figure 1B.

The hydrolysis of the glycosidic bond induced changes in DNA expressed in the overall bending as well as in the local properties around the uracil. The DNA in the complex with UDG is considerably bent as can be seen in Figure 2 as well as from the parameters that describe the inclination (INC, i.e., the angle of the long axis of the base pair) and tip (TIP, i.e., the angle of the short axis) of the base pair and of the local helical axis (AIN and ATP, respectively) (see Figure 3). In standard DNAs, the average INC of the base pair is −5.9° for B-DNA and 19.1° for A-DNA, whereas the TIP parameter for both types of DNA is 0°. The DNA in the complex with UDG has an average INC of −36.5° in both the r- and the p-complex, indicating that the bases are strongly tilted. Moreover, in the r-complex, the connection between uracil and the DNA backbone produces a larger inclination in the U4·G15 base pair of −44.5° compared to −34.6° in the p-complex, as can be seen in Figure 3. The average TIP parameter shows considerably larger tilting in the r-complex, 33.2°, than in the p-complex, 20.8°. Furthermore, in the r-complex, the TIP parameter of the U4·G15 step is very large, 48.7°, but it changes by as much as 56.9° to −8.2° in the p-complex (see Figure 3), suggesting a release of the strained backbone in the r-complex by the hydrolysis of the glycosidic bond. Similar conclusions can be drawn from the axis parameters AIN and ATP shown in Figure 3. In unperturbed DNA, the average structure is generally straight, leading to axis parameters with a value of 0°. However, both average parameters in the complexes are around 10° in AIN and 19° in ATP. Most importantly, the AIN parameters in the U4·G15 step change from 3.7° in the r-complex to −15.0° in the p-complex and the ATP parameter changes from 13.5 to 7.4° (see Figure 3). These changes demonstrate that the level of bending of DNA in the p-complex has been reduced by the hydrolysis of the glycosidic bond.

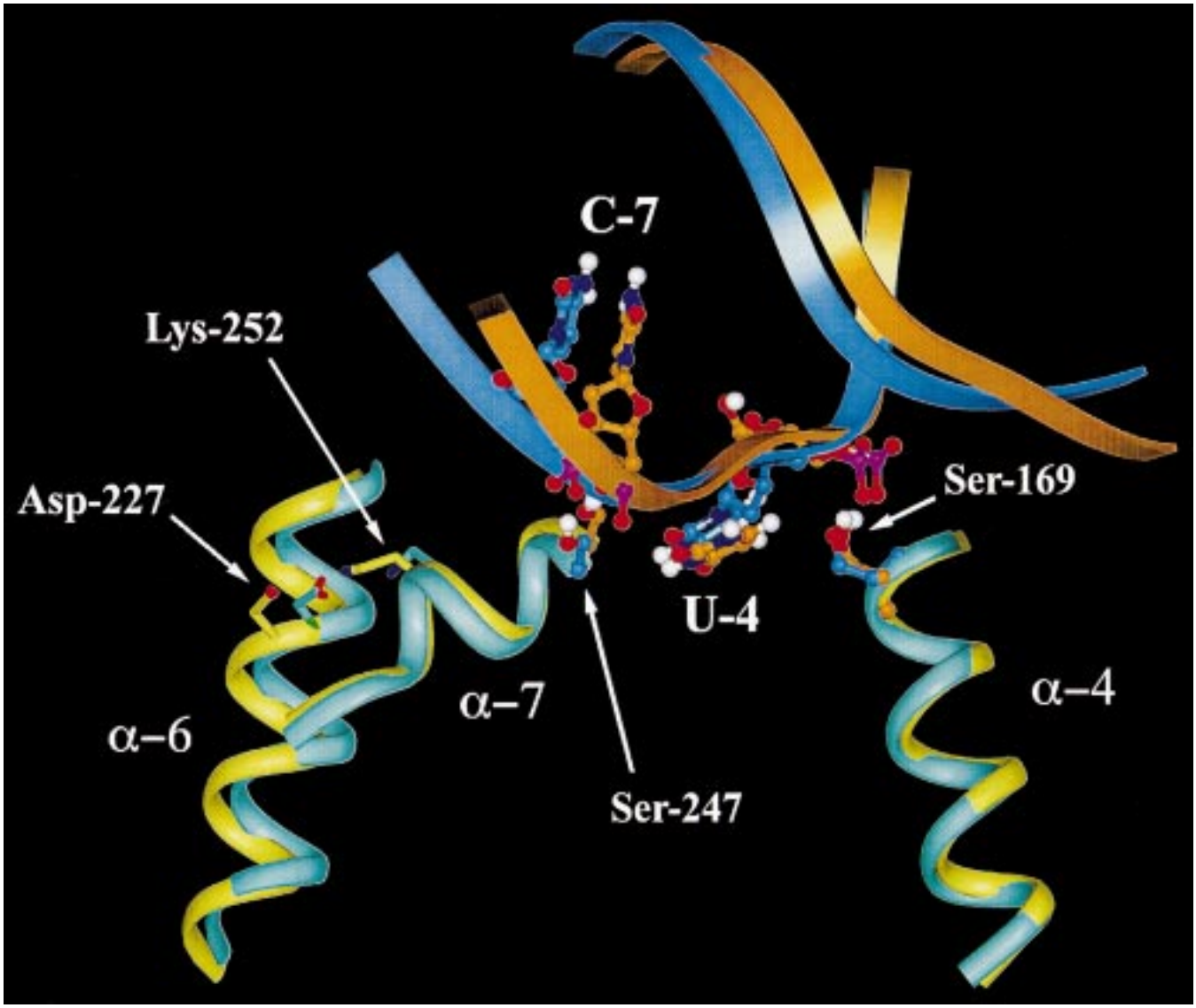

FIGURE 2: Conformational changes in the UDG and DNA backbone upon cleavage of the $N_1-C_{1'}$ glycosylic bond. The r-complex (blue) and p-complex (yellow) structures are fitted by the backbone heavy atoms of UDG. The DNA backbone changes induce the shift of the position of helix α_7 relative to α_4 through two contacting points, Ser-247 and Ser-169, with DNA; the movement of α_7 then turns α_6, through an ionic bridge between Lys-252 and Asp-227.

The backbone torsional angles also report the changes in DNA upon the hydrolysis of the glycosidic bond, and they demonstrate that the changes are localized to the neighborhood of the flipped uracil. These changes are summarized in Table 1. In the r-complex, all angles, except δ, deviate from standard backbone angles as represented by either A- or B-DNA. These deviations represent base flipping and backbone distortion induced by the interaction with the protein. The contribution of base flipping and distortion can be estimated by comparing the DNA torsional angles in the r-complex to those in the p-complex. The p-complex, in which the uracil−sugar bond has been hydrolyzed, can be representative of base flipping alone. This is characterized by large changes in only two angles; γ is rotated by $-148°$ and ϵ by $-101°$ compared to those in B-DNA. In the r-complex, the torsional angles change further because of the additional strain induced by the protein. Thus, α is rotated by 141°, γ by 103°, ϵ by $-146°$, and ζ by 85°. It appears therefore that the UDG induces a significant bending in the DNA, which possibly helps in flipping the uracil into an extrahelical position. However, the glycosidic bond in the substrate state imposes a certain rigidity of the backbone, which is relaxed upon its hydrolysis. This change is illustrated in Figure 2, and shows the retraction of the backbone around U-4 upon hydrolysis of the glycosidic bond, generating essentially a more bent structure of the DNA. The consequences of these changes are also transmitted to the protein as discussed above. Furthermore, the global changes in DNA and protein structure have also a major impact on the local environment in the active site (see below).

Structure of the Binding Pocket. The binding pocket is specific for uracil as has been determined by the X-ray crystallographic structure and by mutational experiments. As determined from X-ray structure (*14*, *15*), the specificity of the pocket comes from its organization around a relatively rigid loop spanned by the backbone from Gln-144 to Tyr-147 and from two hydrophobic residues, Phe-158 and Tyr-147, whose side chains complete the steric boundaries of the binding pocket. In this respect, the binding pocket in the r-complex is very similar to that observed in the crystal structure of the UDG−DNA p-complex. In both structures, the uracil base is stacked on the phenyl ring of Phe-158 on

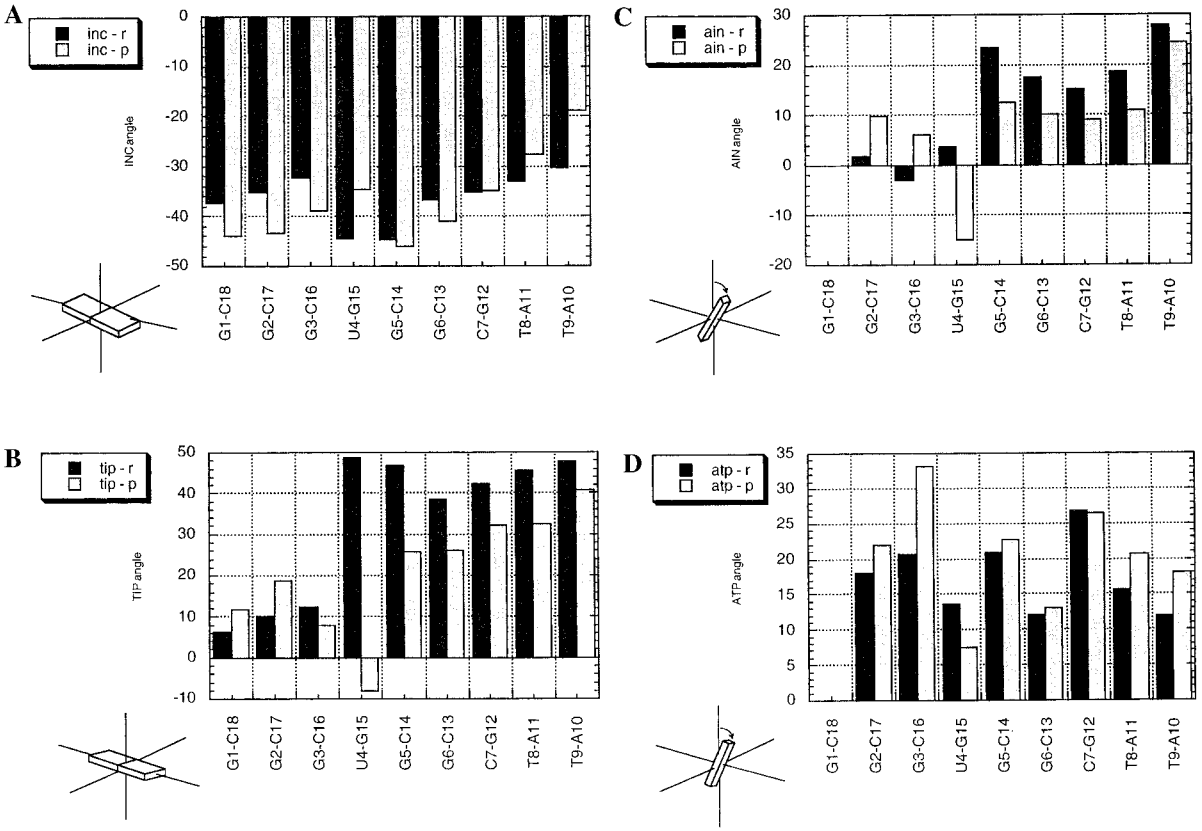

FIGURE 3: Base pair parameters in the r-complex and in the p-complex: (A) inclination (INC), (B) tip (TIP), (C) axis angle in inclination (AIN), and (D) axis angle in tip (ATP).

Table 1: Torsional Angles of the DNA Backbone Near Uracil

	α (deg)	β (deg)	γ (deg)	δ (deg)	ϵ (deg)	ζ (deg)
r-complex	173	165	293	159	301	229
p-complex	283	157	184	143	256	298
A-DNA	285	208	45	83	178	285
B-DNA	314	214	36	156	135	314

one side and constrained on the other side by the backbone arch. Tyr-147 is nearly perpendicular to the base on the side of the C_5-C_6 bond, precluding access to thymine by blocking bulky substitutions on these atoms.

In addition to the steric selectivity, the crystal structures show that several hydrogen bonds contribute to specificity through polar interactions. The O_4 of uracil forms a H-bond with the backbone NH of Phe-158 and the O_2 with that of Gln-144. These H-bonds are maintained in both simulations of the r- and p-complex. On the basis of the crystal structure, the selectivity toward uracil and the exclusion of cytosine has been attributed to a double H-bond between the side chain of Asn-204 on one hand and the O_4 and N_3H of uracil on the other hand. In agreement with the crystal structure, the double hydrogen bond is maintained throughout the simulation in the p-complex. However, in the r-complex the O_δ(Asn-204)$\cdots$HN$_3$(U) H-bond is intact for 100% of the simulation, whereas the N_δH(Asn-204)$\cdots$O$_4$(U) H-bond is only maintained for 20% of the time. Examination of the trajectory of the r-complex shows that after an initial period of 200 ps, during which the double H-bond was maintained, it was interrupted for 850 ps and fluctuated between a bound and unbound state for the rest of the simulation. In the configurations with the disrupted H-bond, the NH_2 group of Asn-204 forms H-bonds with the backbone carbonyls of Gln-144 and Val-206 while O_4 of uracil engages 100% of the time in an H-bond with H_2O-334 in the cavity behind the binding pocket of uracil. This water is tightly held by three other H-bonds to the NH of Tyr-147, the OH of H_2O-317, and the O of H_2O-341.

The crystal structure of the UDG−DNA p-complex shows that the cavity that binds uracil is extended into the interior of the protein past a narrow passage defined by the backbone of Cys-157 and Phe-158. Three water molecules have been identified in this cavity in the human UDG−DNA complex (*14*). The crystal structure of the viral UDG with a uracil base in the binding pocket shows five structural water molecules in the same cavity (*7*). We have examined the behavior of the waters in the internal pocket based on MD simulations of both the r- and the p-complex. The simulation of the p-complex started from the UDG−DNA crystal structure with the three structural waters in the cavity surrounded with water molecules in the periodic box. After 400 ps, the number of water molecules in the region behind the uracil increased from three to five and remained stable throughout the rest of the simulation of the p-complex. Since the r-complex simulation started from the equilibrated structure of the p-complex, these five water molecules remained in the cavity also for the r-complex throughout the simulation. The simulations do not provide additional information about the lifetime of the waters in this cavity, but it is clear that they must exceed 1.5 ns because they did not exchange during the course of the simulation. Figure 4 is an example of a snapshot that shows the organization of the waters in the cavity inside the enzyme. The figure shows a view of the cavity behind the uracil from a vantage point outside the enzyme. To expose the waters in this cavity, the

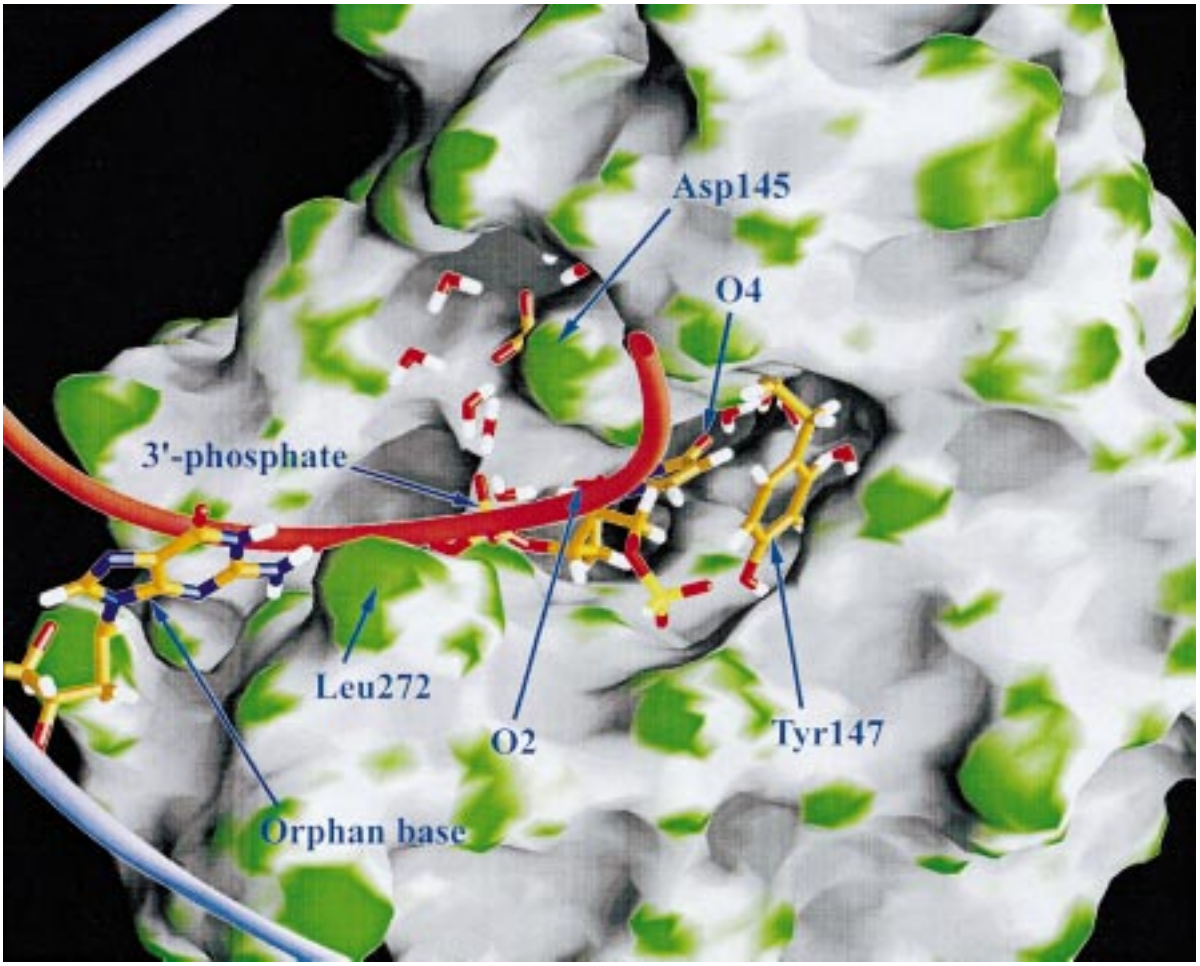

FIGURE 4: Organization of the uracil binding pocket and the proximal active site residues in the enzyme−DNA complex derived from a simulation snaphsot of the r-complex. The vantage point is from the side of the DNA bound to the enzyme. To expose the cavity that contains waters behind the binding pocket of uracil, the molecular surface of Tyr-147 has been removed and the details of the DNA have been hidden. The DNA backbone is represented by the pink and the light blue tubes that contain the flipped uracil and the orphan base, respectively. Only four waters can be seen in the cavity behind the uracil; the fifth water is obstructed by the surface of the protein. On the left of the binding pocket, the water structure around Asp-145 and the 3′-phosphate can be seen. A snaphsot of only the first solvation layer around these residues is shown. For a detailed analysis of the water structure around the active site residues, see the text.

molecular surface of Tyr-147 had to be removed and the details of the DNA had to be hidden. Only four waters can be seen because one water is obstructed from view by the surface of the protein. Among the five waters, two are tightly bound and can be identified with those observed in the crystal structure. One water makes hydrogen bonds with the carbonyl oxygens of Leu-156 and Ser-159 as hydrogen donors and with the backbone NH of His-154 as a hydrogen acceptor. The other water forms a hydrogen bond with the carbonyl oxygen of Gly-155 and the backbone NH of Asn-204. The other three water molecules are mobile inside the cavity, and their hydrogen bonding partners change along the trajectory. They include the backbone and side chain amide of Asn-204, backbones of Tyr-147, Leu-202, Val-206, and Leu-207, and O_4 of uracil, in addition to the groups H-bonded to the two tightly bound waters. The role of these waters in enzymatic catalysis or in substrate recognition is not clear. Considering that the hydrogen bond network formed by these five water molecules in the cavity behind Cys-157 is stable over a considerable period of time, we can treat it as an integral part of the enzyme structure with special hydrophilic properties.

Catalytic Residues. Two residues, Asp-145 and His-268, have been identified as essential for catalytic activity. Mutation of Asp-145 to Asn reduces the specific activity to 0.04% of the wild-type value, suggesting that the negative charge of the carboxylate is important. However, the mutation Asp145Glu also reduces the activity of the enzyme to 0.08% of the native value, suggesting that the effect of this residue is not simply an electrostatic effect due to the negative charge of the carboxylate. Mutation of His-268 to Leu also reduces the enzyme activity to 0.3% of the wild-type value, indicating its importance in the catalytic step. As indicated by the crystal structure, His-268 is also part of the binding pocket of the p-complex, forming an additional H-bond to O_2 of uracil. The analysis of the trajectories of the r- and p-complexes sheds a new light on the catalytic roles of these two residues.

His-268. The H-bond between His-268 and O_2 of uracil is maintained in the simulation of the p-complex at an average distance of 2.25 Å, in full agreement with the crystal structure. However, it is disrupted in the r-complex as indicated by the increase in the distance between His-268 and O_2. An examination of the trajectory of the r-complex shows that the average distance between $H_{\epsilon 2}$ of His-268 and O_2 of uracil is 3.45 ± 0.34 Å, and it is clearly too long for a direct H-bond. The displacement of His-268 is due to the approach of deoxyribose to the uracil upon reconstruction

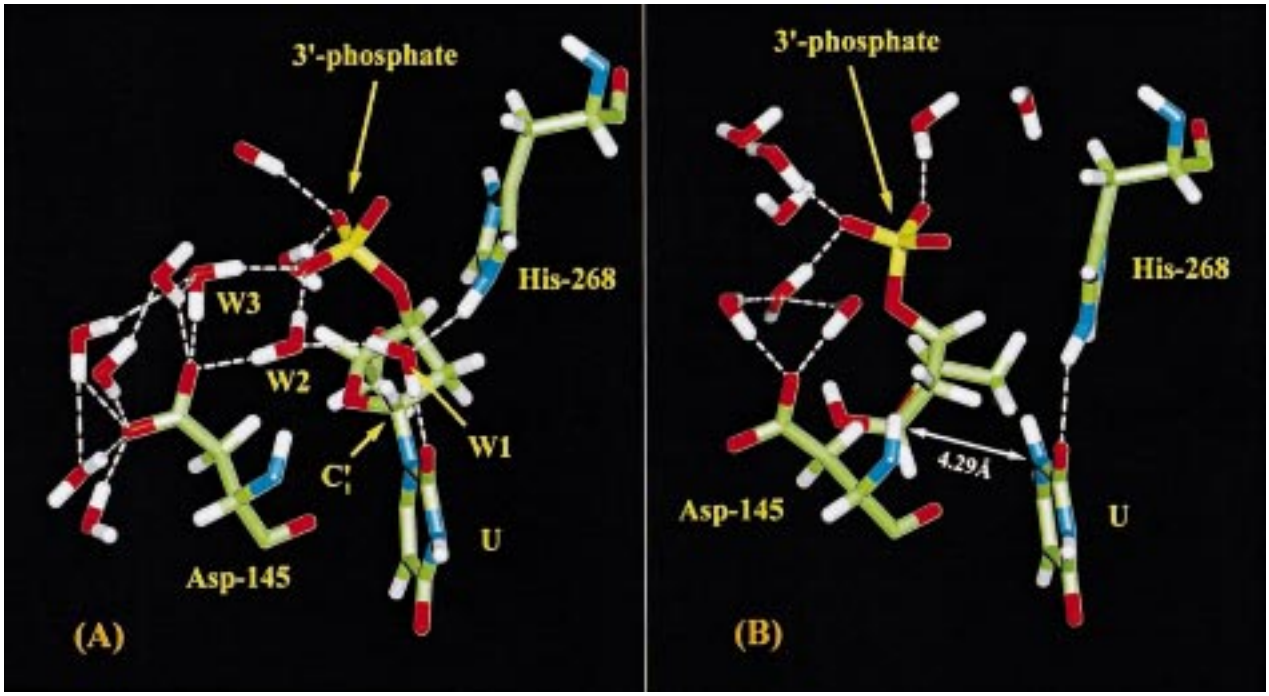

FIGURE 5: Simulation snaphsot of the catalytic center around His-268, Asp-145, and uracil with the 3′-phosphate in the r-complex (A) and the p-complex (B). His-268 in the r-complex, shown in a protonated form, is bridged to O_2 of uracil through a water molecule (W1) which H-bonds to both sides. Two water molecules (W2 and W3) can be identified in the r-complex bridging Asp-145 and the 3′-phosphate. The other waters constitute the rest of the first solvation layer. In the p-complex, His-268 moves to form a close H-bond with uracil. The movement of the sugar with the 3′-phosphate disrupts the tight bridge to Asp-145. For details, see the text.

Table 2: pK_a Values of His-268 and Asp-145

	His-268	Asp-145
UDG	4.93 ± 0.55	4.14 ± 0.21
UDG−DNA r-complex	7.13 ± 0.60	4.35 ± 0.12
UDG−DNA p-complex	5.48 ± 1.00	3.02 ± 0.54

of the glycosidic bond in the r-complex. This change is illustrated in Figure 5. In both the crystal and MD structures of the UDG−DNA p-complex (Figure 5B), His-268 is well within H-bonding distance. However, as can bee seen in Figure 5A, such a position for His-268 is impossible in the r-complex because the $C_{2'}$ methylene group of the deoxyribose presents a steric obstacle for the approach of His-268 to the uracil. The space left by the dislocation of His-268 becomes occupied by a water molecule (W1 in Figure 5), which becomes locked between $H_{\epsilon 1}$ of His-268 and O_2 of the uracil base after about 200 ps of the simulation and stays there throughout the rest of the 1.4 ns simulation. The water has some rotational freedom in this position as indicated by the occasional interchanges of orientation of its two hydrogens, while maintaining the bridging hydrogen bonds to His-268 and uracil.

The change in the environment of His-268 suggested that the protonation state of this residue may change during the course of the enzymatic reaction. We have calculated the pK_a of His-268 in the r- and p-complexes as well as in the free enzyme (Table 2). The calculated pK_a of His-268 in the free enzyme is 4.9 ± 0.5, but upon formation of the r-complex, the pK_a increases to 7.1 ± 0.6. Examination of the contributions to the change in pK_a shows that the major part comes from the electrostatic effects of the environment. The insertion of a water molecule between His-268 and the uracil as well as the proximity of the negatively charged DNA stabilizes the protonated form of the imidazole by 3 kcal/mol and is expressed in the increased pK_a. The hydrolysis of the glycosidic bond produces a large change in the pK_a of His-268, lowering it back to 5.5 ± 1.0 in the p-complex. An examination of the effects on pK_a shows that the elimination of the water that was bridging His-268 and O_2 of uracil is largely responsible for the lowering of the pK_a in the p-complex. The conformational changes in the DNA produced by the hydrolysis of the glycosidic bond may also contribute to the lowering of the pK_a of His-268 in the p-complex by retracting the DNA backbone from its distorted form.

The role of His-268 in catalysis as it emerges from the simulations is somewhat different from the mechanism that was proposed on the basis of the crystal structure. His-268 in the free enzyme is neutral as indicated by its low pK_a, but in the substrate−enzyme complex (the r-complex), the pK_a of His-268 increases above 7 due to the bridging water and the proximity of the negative field produced by the DNA. Thus, His-268 does not act directly as a positively charged group to stabilize the negative charge that develops on uracil in the course of glycosylase action. Rather, it activates a water molecule to act as a proton donor or a proton shuttle from His-268 to the uracil during the course of the hydrolysis. In the enzyme−product complex (p-complex), the pK_a of His-268 is reduced back to 5.5, indicating that at the end of the enzymatic reaction His-268 becomes neutral, enhancing the release of the products possibly because of a weakened H-bond to uracil.

Asp-145. Another important residue for enzymatic catalysis is Asp-145 as indicated by the effect of its mutation on catalysis. It has been proposed that Asp-145 acts as a general base that abstracts a proton from a water molecule and forms the nucleophile OH^-. For such a process to be enzymatically effective, the pK_a of Asp-145 should be significantly higher

than of aspartic acid in solution. In the crystal form, Asp-145, because it has been mutated to Asn, has its side chain oriented toward the uracil base and is close to the $C_{1'}$ position in the UDG−DNA complex. Thus, from the crystal structure of the human double mutant UDG−DNA complex, it is difficult to assess the role of Asp-145 not only because it has been mutated but also because the complex represents the product stage of the reaction. As has been discussed above, speculating about the catalytic mechanism from the product stage of the reaction could lead to erroneous conclusions We have therefore analyzed the properties of this residue on the basis of the simulations of the r- and p-complexes.

The replacement of the Asn with the negatively charged Asp reorients the side chain away from the uracil base into the aqueous environment that separates the DNA from the protein. In the r-complex, this orientation of the side chain of Asp-145 is fixed throughout the simulation because the carboxylate forms a stable H-bond to a water molecule (W2 in Figure 5) that in turn forms a stable H-bond with the 3′-phosphate to the uracil. The distribution of distances between the 3′-phosphate and the carboxylate of Asp-145 extracted from the simulation of the r-complex confirms this observation. The average distance between $O_{\delta 2}$ of Asp-145 and the O_{1P} of the 3′-phosphate is 3.85 ± 0.26 Å, indicating that the two groups, while not in direct contact, are held almost in a rigid configuration by the intervening water molecule. An analysis of the water around the carboxylate of Asp-145 shows that on the average the number of waters in the first solvation shell (R_{sh} = 3.55 Å) is 6.33 ± 0.72. Similarly, the coordination within 3.4 Å around the 3′-phosphate is 4.61 ± 0.63 water molecules. Most importantly, the combined coordination number around $O_{\delta 2}$ of Asp-145 and O_{1P} of the 3′-phosphate is 2.04 ± 0.54 water molecules. Inspection of the water structure around Asp-145 and the 3′-phosphate (Figure 5A) shows that two water molecules form a bridge between $O_{\delta 2}$ and O_{1P}, but while one (W2) is stable, the other (W3) exchanges on a time scale of approximately 0.5 ns. This arrangement is unique to the r-complex and is made possible by the presence of the glycosidic bond, which brings the 3′-phosphate close to the carboxylate of Asp-145. In contrast, in the p-complex the distribution of distances between Asp-145 and the 3′-phosphate becomes much wider and its selectivity for $O_{\delta 1}$ versus $O_{\delta 2}$ of Asp-145 is lost. The average distance between $O_{\delta 1}$ and O_{1P} is 6.35 ± 0.61 Å, and that between O_{1P} and $O_{\delta 2}$ is 7.31 ± 0.66 Å. The increase in the distance and the loss of orientational selectivity of Asp-145 are the consequence of the hydrolysis of the glycosidic bond and the subsequent displacement of the deoxyribose and the 3′-phosphate that is attached to it away from Asp-145. Analysis of the water structure shows a significant change in the coordination around Asp-145 and the 3′-phosphate. The carboxylate of Asp-145 becomes partially buried as indicated by the presence of only 2.22 ± 0.77 water molecules around it. The solvation of the 3′-phosphate on the other hand has not changed significantly, with 3.98 ± 0.88 waters in the first solvation shell. Because of the increase in the distance between Asp-145 and the 3′-phosphate, only 0.16 ± 0.37 water is shared between them. Thus, although more waters can be found in the space between these groups in the p-complex, none of them are shared as intimately as the two waters in the r-complex. This change is important to the catalytic mechanism (see below).

The extensive solvation of Asp-145 raises the question of whether it could act as a general base for the abstraction of a proton from a water molecules in forming the nucleophile for the hydrolytic reaction. We have calculated the pK_a of this residue in the free enzyme as well as in the r- and p-complexes (Table 2). In the free enzyme, the pK_a of Asp-145 is 4.1 ± 0.2, in agreement with its position on the surface of the protein. This value is not significantly different from a free aspartic acid in aqueous solution. In the r-complex, the pK_a of Asp-145 only increases to 4.4 ± 0.1, which is consistent with the approach of the negatively charged DNA. However, because the carboxylate remains nearly fully solvated even in the r-complex, the pK_a increases only by a small amount. In the p-complex, the pK_a of Asp-145 is lowered to 3.0 ± 0.5 because it interacts directly with Lys-218 in the loop that connects $\beta_{2'}$ and helix α_6. This loop does not interact directly with DNA, but its position is determined by the interaction of Ser-247 at the top of helix α_7 and the phosphate of Cyt-7 in the DNA (see above). In the r-complex, Lys-218 is 4.4 Å away from Asp-145 and it interacts with it through a water molecule. The number of water molecules within 3.5 Å of the NH_3^+ of Lys-218 is 2.64 ± 1.28, but only 0.81 water is shared with Asp-145. The screening of the positive charge through a water maintains a normal pK_a of both residues and is not restraining the motion of the loop as indicated by a large rms deviation around the average (see Figure 1B). As described previously, the changes in DNA after the hydrolysis of the glycosidic bond cause the change in the positions of the α_7 and α_6 helices through the ionic interactions of Asp-227 and Lys-252. As helix α_6 rotates it also repositions the loop between $\beta_{2'}$ and α_6, moving N_ζ of Lys-218 by 3.23 Å toward Asp-145. This movement displaces the water molecule that bridged Asp-145 and Lys-218 and produces a salt bridge that rigidifies the loop, as can bee seen in Figure 1A. The proximity of a positive charge near the Asp-145 also lowers its pK_a.

Thus, it appears that the pK_a of Asp-145 is too low to act as a general base to induce a proton abstraction to form the hydroxide anion. Moreover, the juxtaposition of the negatively charged 3′-phosphate on the other side of the water molecule near Asp-145 also prevents a proton transfer from the water to either the carboxylate or the phosphate. Positioning a negative charge (i.e., the phosphate) in the proximity of a water molecule that is already H-bonded to a negative group (i.e., the carboxylate) reduces the probability of a proton transfer because of electrostatic reasons. This can be restated in terms of distances between the negative species before and after proton transfer. Before proton transfer, the water is separating the negative charges to a distance of 3.85 Å. The proton transfer either to the carboxylate or to the phosphate will reduce the distance between the negatively charged groups (i.e., hydroxide and phosphate or carboxylate) to a distance of ∼3.0 Å. The concomitant increase in electrostatic repulsion will act against this process. Therefore, the role of Asp-145 in UDG catalysis must be redefined.

A Proposed Catalytic Mechanism. The proposed mechanism for UDG catalysis is presented in Figure 6. The mechanism is based on results derived from MD simulations of the r- and the p-complexes which exhibit significant

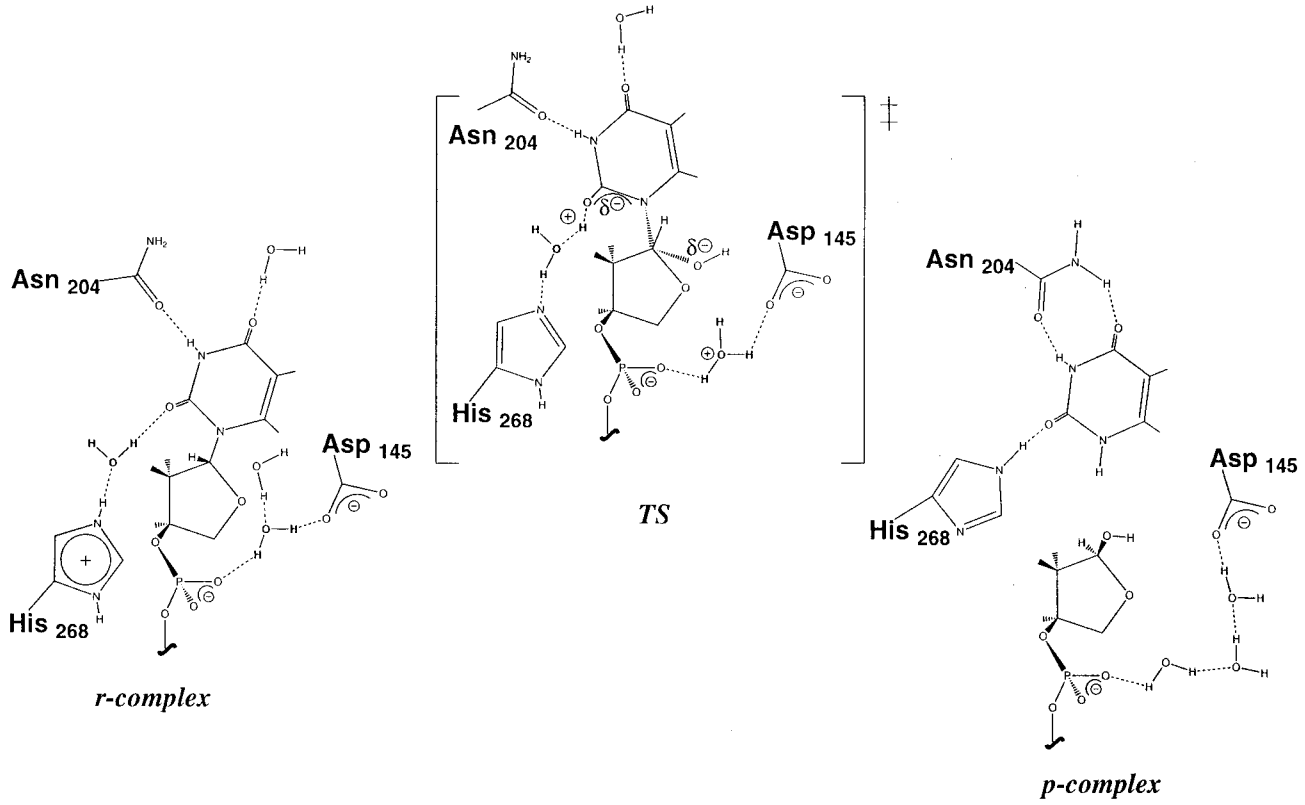

FIGURE 6: Schematic representation of a proposed mechanism for UDG catalysis.

differences in three sites around the uracil. The structure and properties of the p-complex derived from the simulations are in very good agreement with the crystal structure, lending credence to the simulation protocol. Using the same simulation method, we find in the r-complex organized waters near O_4 of the uracil base, bridging O_2 and His-268 as well as the 3′-phosphate of the flipped-out nucleotide and Asp-145. These waters do not exist in such an organized form in the p-complex, and we suggest that they play an important role in catalysis.

The first difference is the disruption of the H-bond between the NH_2 group of Asn-204 and O_4 and the substitution of this H-bond donor with a specific water from the five waters trapped in the pocket behind the uracil. This configuration is quite steady in our simulation, providing a stable H-bond for nearly 80% of the 1.4 ns simulation time. It is supported by a network of H-bonds to the other five waters in the cavity as well as to specific side chain and main chain groups in the pocket (see above). The other source of support is a stable H-bonding of the NH_2 group of Asn-204 to the backbone carbonyls of Gln-144 and Val-206. The significance of this arrangement for catalytic activity is not clear at the present time. However, several water molecules are also found in the same area in the G·T/U mismatch-specific DNA glycosylase (MUG) (*29*) even though the Asn-204 that is conserved in different UDGs has been replaced with a Lys in MUG. Also, the mutation of Asn-204 to Asp has a relatively small effect on K_M (only a factor of 24) but a very large effect on k_{cat} (a factor of more than 2000). Thus, it appears that a proper polar environment generated by the waters near O_4 of uracil is essential for an effective stabilization of the transition state.

The second difference is localized around His-268 where a water molecule is present between O_2 of uracil and N_ϵ of His-268. The presence of the water is primarily due to the steric repulsion of His-268 exerted by the deoxyribose, but its effect on the ionization properties of His-268 is very profound. It increases the pK_a of the imidazole from 5.9 in the free enzyme to 7.1 in the r-complex, effectively converting it to a protonated histidine. In this form, His-268 can either stabilize the developing negative charge in the transition state or donate a proton via the bridging water to complete the hydrolysis. The retraction of the backbone after the hydrolysis of the glycosidic bond removes the steric obstacle presented by the sugar, allowing a close approach of the imidazole to form a direct H-bond with the uracil. The removal of the water also lowers the pK_a of His-268 to 6.1, effectively allowing it to donate the proton to the hydrolyzed uracil.

Perhaps the most important difference between the r- and the p-complexes is in the immobilization of two water molecules between Asp-145 and the 3′-phosphate to uridine. These waters form a relatively long-lived (>1 ns) arrangement bridging two negatively charged groups, which come from the enzyme (Asp-145) and the substrate (3′-phosphate). The interface between the protein and the DNA in the UDG−DNA complex remains largely solvated, maintaining an almost full hydration shell of the two negative groups. It has been proposed that Asp-145 acts as a general base catalyst to prepare the hydroxide anion through a proton abstraction from water. Subsequently, this anion performs the nucleophilic substitution reaction that results in the hydrolysis of the glycosidic bond. The overall activation energy that translates to the observed k_{cat} can be divided into two contributions; one is the free energy needed to prepare the hydroxide anion from water (ΔG_H), and the second is the free energy of activation ($\Delta g^{\ddagger}$) of the nucleophilic substitution. The first contribution can be evaluated by

comparing the pK_a of Asp-145 in solution and in the enzyme. It would be expected that for the enzyme to lower the barrier by stabilizing the OH^-, the pK_a of Asp-145 should increase. The calculated pK_a of Asp-145 in the r-complex is around 4.1, which is not different from its value in aqueous solution. On the basis of the extensive solvation of the interface between the enzyme and the DNA, it is also reasonable to assume that the pK_a of the 3′-phosphate should not change from its value in solution. Thus, on the basis of only pK_a considerations, these groups cannot act as a general base catalyst because they do not provide any stabilization of the hydroxide anion compared to an aqueous solution. Furthermore, on the basis of electrostatic considerations, an arrangement in which a water molecule bridges two negative charges is also not conducive to stabilizing a hydroxide group. A transfer of a proton from water to any of the negatively charged groups will bring the negative charges closer to each other and therefore will result in increased electrostatic repulsion instead of a stabilization. Thus, the particular arrangement observed in the r-complex cannot provide a reduction in ΔG_H because it does not stabilize the proton transfer process.

We propose an alternative mechanism in which the enzyme can stabilize the hydroxide anion. In this mechanism, a proton transfer occurs between the two water molecules that are bridging the Asp-145 and the 3′-phosphate (Figure 6). Transfer of a proton from one water molecule to the other produces a hydronium ion and a hydroxide. The hydronium ion stabilizes the close juxtaposition of the negative charges of Asp-145 and the 3′-phosphate, and the resulting hydroxide can serve as the nucleophile as shown in the TS diagram (Figure 6). This mechanism presents a plausible pathway for reducing the ΔG_H and for contributing to the lowering of the barrier. A separate issue is the lowering of $\Delta g^{\ddagger}$ by stabilization of the transition state. This requires the knowledge of the structure of the TS and will have to be investigated with a combined quantum mechanical/molecular mechanical approach. Nevertheless, already at the present stage, it can be proposed that His-268 through its changes in pK_a and the introduction of a water molecule next to O_2 of uracil can stabilize the charge-separated transition state. Also, it appears that the water molecules buried in the interior of the protein behind the uracil could also contribute to the stabilization of the transition state. These factors will be investigated in future work.

The completion of the enzymatic reaction is accomplished in several sites upon hydrolysis of the glycosidic bond (Figure 6). The retraction of the DNA backbone upon hydrolysis moves the sugar and allows a formation of a stable H-bond between His-268 and uracil by releasing the intervening water. This also changes the pK_a of His-268 to allow transfer of a proton to N_1 of uracil. Together with the backbone, the phosphate moves a further distance away from the carboxylate and changes the nature of the bridging water to that of the bulk solvent. The concomitant changes in the protein also anchor the side chain of Asp-145 in an ionic interaction with Lys-218. Finally, small changes in the binding pocket of uracil form the double H-bond between Asn-204 and uracil and remove the water that was H-bonded to O_4. The molecular details of the proposed mechanism will be tested explicitly in future studies.

The proposed mechanism assigns specific roles to the residues in the binding pocket and in the active site and clarifies the participation of water molecules in the catalytic reaction. When the fact that the reaction in water has a very large barrier of ~30 kcal/mol (*30*) is considered, the enzyme manages to lower the barrier for the hydrolysis of the glycosidic bond to approximately 15 kcal/mol. Such a remarkable change in the barrier, which translates to approximately 10 orders of magnitude of enhancement in the rate constant, must be accomplished in part by stabilization of the proton transfer and in part by stabilization of the transition state. Further studies will be required to evaluate the relative contributions of the enzyme to each of the stabilization components.

ACKNOWLEDGMENT

We thank Dr. John Tainer for providing the coordinates of the UDG−DNA complex.

REFERENCES

1. Lindahl, T. (1993) *Nature 362*, 709−715.
2. Prolla, T. A., Baker, S., and Liskay, R. M. (1998) in *Genetics of DNA Mismatch Repair, Microsatellite Instability, and Cancer* (Prolla, T. A., Baker, S., and Liskay, R. M., Eds.) Vol. 2, pp 443−464, Humana Press Inc., Totowa, NJ.
3. Lindahl, T. (1974) *Proc. Natl. Acad. Sci. U.S.A. 71*, 3649−3653.
4. Mol, C. D., Arvai, A. S., Sanderson, R. J., Slupphaug, G., Kavli, B., Krokan, H. E., Mosbaugh, D. W., and Tainer, J. A. (1995) *Cell 82*, 701−708.
5. Mol, C. D., Arvai, A. S., Slupphaug, G., Kavli, B., Alseth, I., Krokan, H. E., and Tainer, J. A. (1995) *Cell 80*, 869−878.
6. Savva, R., and Pearl, L. H. (1995) *Nat. Struct. Biol. 2*, 752−757.
7. Savva, R., McAuley-Hecht, K., Brown, T., and Pearl, L. (1995) *Nature 373*, 487−493.
8. Winters, T. A., Henner, W. D., Russell, P. S., McCullough, A., and Jorgensen, T. J. (1994) *Nucleic Acids Res. 22*, 1866−1873.
9. Matsumoto, Y., and Kim, K. (1995) *Science 269*, 699−702.
10. Burgers, P. M. (1998) *Chromosoma 107*, 218−227.
11. Lehman, I. R. (1974) *Science 186*, 790−797.
12. Parikh, S. S., Mol, C. D., and Tainer, J. A. (1997) *Structure 5*, 1543−1550.
13. Savva, R., and Pearl, L. H. (1993) *J. Mol. Biol. 234*, 910−912.
14. Slupphaug, G., Mol, C. D., Kavli, B., Arvai, A. S., Krokan, H. E., and Tainer, J. A. (1996) *Nature 384*, 87−92.
15. Parikh, S. S., Mol, C. D., Slupphaug, G., Bharati, S., Krokan, H. E., and Tainer, J. A. (1998) *EMBO J. 17*, 5214−5226.
16. Kavli, B., Slupphaug, G., Mol, C. D., Arvai, A. S., Peterson, S. B., Tainer, J. A., and Krokan, H. E. (1996) *EMBO J. 15*, 3442−3447.
17. Varshney, U., and van de Sande, J. H. (1991) *Biochemistry 30*, 4055−4061.
18. Purmal, A. A., Wallace, S. S., and Kow, Y. W. (1996) *Biochemistry 35*, 16630−16637.
19. Degano, M., Almo, S., Sacchettini, J., and Schramm, V. (1998) *Biochemistry 37*, 6277−6285.
20. Warshel, A. (1981) *Biochemistry 20*, 3167−3177.
21. Bashford, D., and Karplus, M. (1990) *Biochemistry 29*, 10219−10225.
22. Bashford, D., and Karplus, M. (1991) *J. Phys. Chem. 95*, 9556−9561.
23. Mehler, E. (1996) *J. Phys. Chem. 100*, 16006−16018.
24. Mehler, E. L., and Guarnieri, F. (1999) *Biophys. J.* (in press).

25. Brooks, B. R., Bruccoleri, R. E., Olafson, B. D., States, D. J., Swaminathan, S., and Karplus, M. (1983) *J. Comput. Chem. 4*, 187−217.
26. MacKerell, A. D. J., Bashfod, D., Bellot, M., Dunbrack, R. L. J., Field, M. J., Fischer, S., Gao, J., Guo, H., Ha, S., Joseph, D., Kuchnir, L., Kuczera, K., Lau, F. T. K., Mattos, C., Michnick, S., Ngo, T., Nguyen, D. T., Prodhom, B., Roux, B., Schlenkrich, M., Smith, J., Stote, R., Straub, J., Wiorkiewicz-Kuczera, J., and Karplus, M. (1992) *Biophys. J. 6*, A143.
27. MacKerell, A. D. J., Wiorkiewicz-Kuczera, J., and Karplus, M. (1995) *J. Am. Chem. Soc. 117*, 11946−11975.
28. Ehrenson, S. (1989) *J. Comput. Chem. 10*, 77−93.
29. Barrett, T. E., Savva, R., Panayotou, G., Barlow, T., Brown, T., Jiricny, J., and Pearl, L. H. (1998) *Cell 92*, 117−129.
30. Shapiro, R., and Kang, S. (1969) *Biochemistry 8*, 1806−1810.

BI990262H